**Supporting information for**

# Efficient Water Oxidation Using Nanostructured α-Nickel-Hydroxide as an Electrocatalyst

Minrui Gao, Wenchao Sheng, Zhongbin Zhuang, Qianrong Fang, Shuang Gu, Jun Jiang, Yushan Yan*

Department of Chemical and Biomolecular Engineering, Center for Catalytic Science and Technology, University of Delaware, Newark, DE 19716 USA

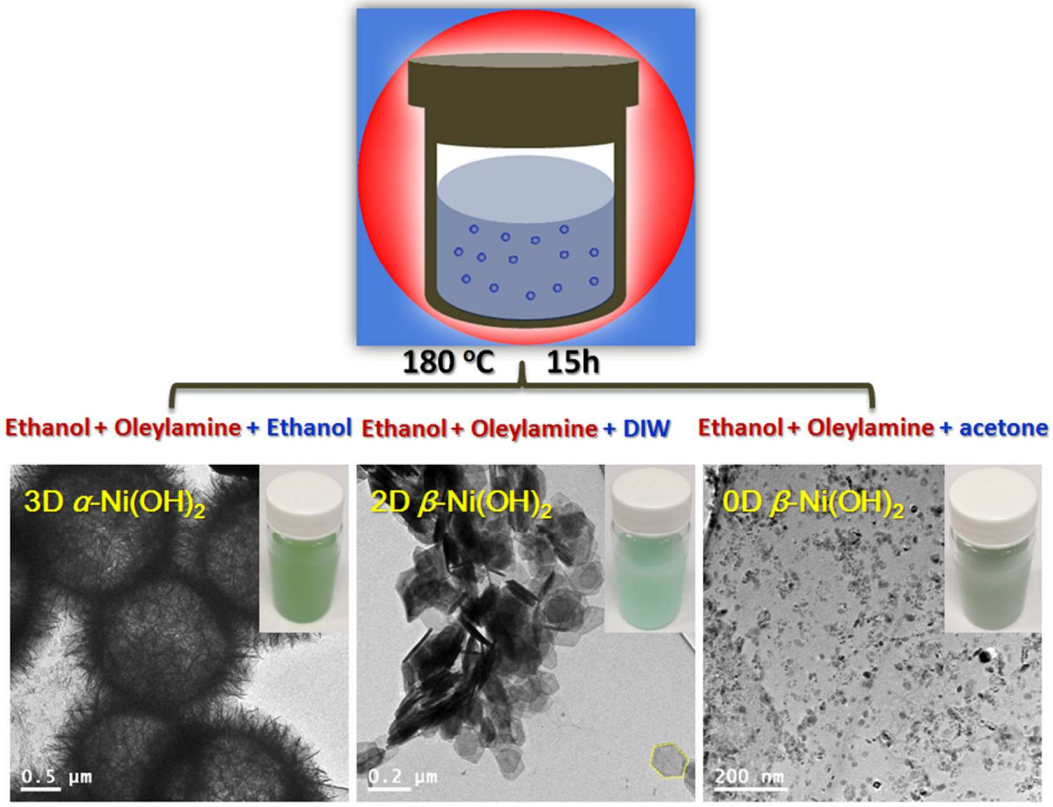


Figure S1. Schematic of the preparation of nanosheet-assembled $\alpha$-$Ni(OH)_2$ hollow spheres (Left), $\beta$-$Ni(OH)_2$ hexagonal nanoplates (Middle), and $\beta$-$Ni(OH)_2$ nanoparticles (Right) by a facile solvothermal method. Insets show corresponding digital photographs of the as-prepared nanostructures dispersed in ethanol.

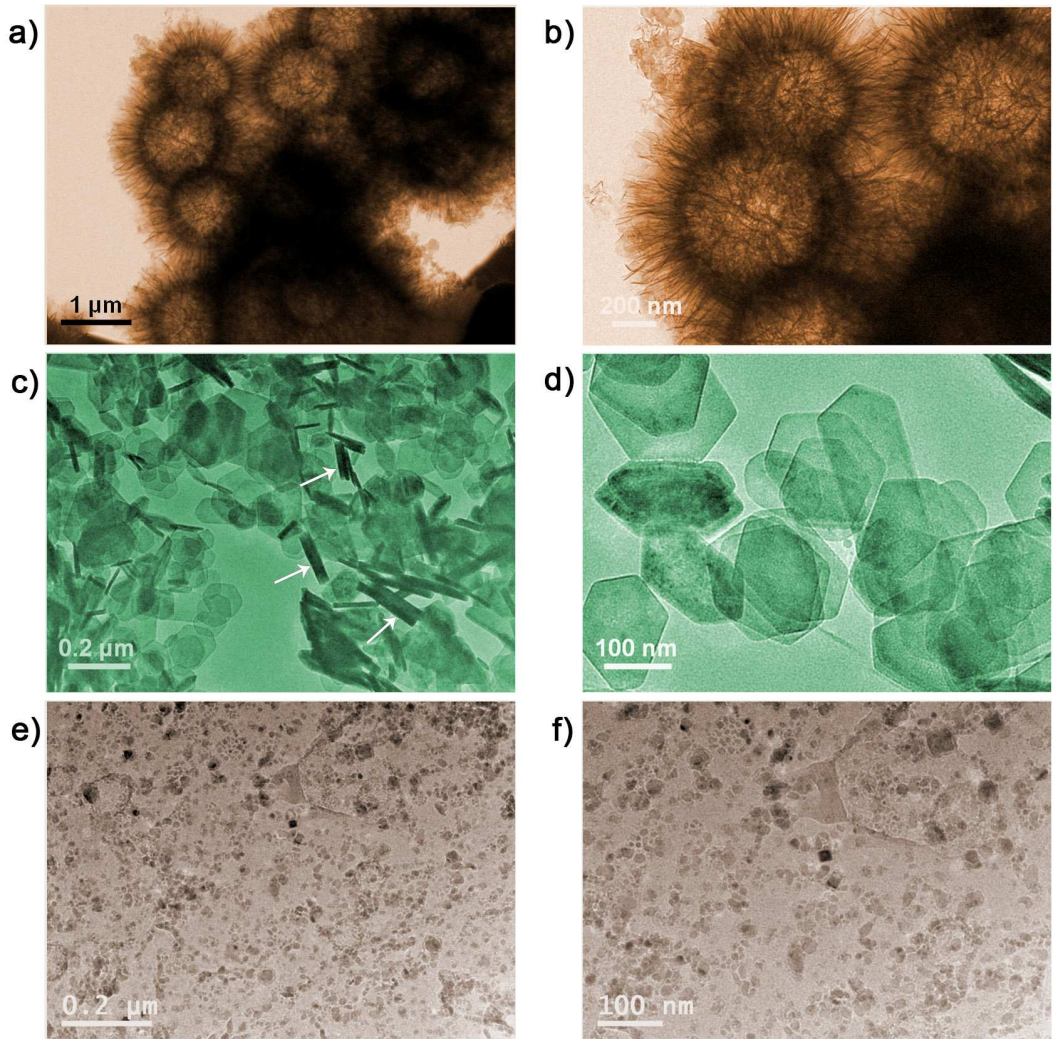


Figure S2. TEM images with different magnifications for $\alpha$-$Ni(OH)_2$ hollow spheres (a, b); $\beta$-$Ni(OH)_2$ nanoplates (c, d); and $\beta$-$Ni(OH)_2$ nanoparticles (e, f), respectively. White arrows in (c) point out the assembly of $\beta$-$Ni(OH)_2$ nanoplates perpendicular to the TEM grid.

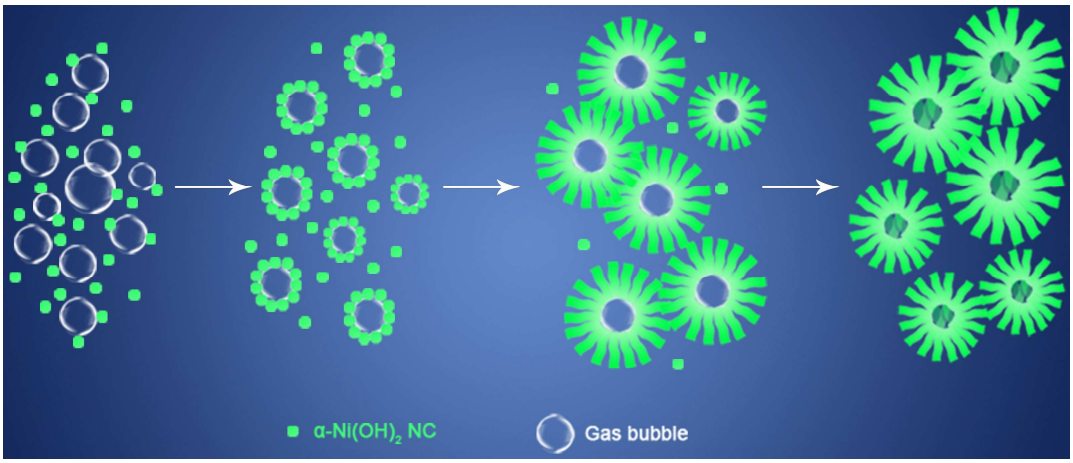


Figure S3. Schematic of the proposed formation mechanism of the nanosheet-assembled $\alpha$-$Ni(OH)_2$ hollow spheres.

A gas bubbles-assisted soft template process is proposed for the formation of $\alpha$-$Ni(OH)_2$ hollow spheres (see Figure S3). Under solvothermal environment at 180 $^{o}$C, the boiling reaction solution (*i.e.*, ethanol and oleylamine) can generate stable emulsions and foams. The newly formed tiny $\alpha$-$Ni(OH)_2$ crystal nucleus may attach on the gas/liquid interface. Owing to its nature of lamellar 2D structures, $\alpha$-$Ni(OH)_2$ (a layered structure of the $CdI_2$ type) prefers to grow along the layered plane,[S1] leading to sheet-like nanostructures instead of nanoparticles. These $\alpha$-$Ni(OH)_2$ nanosheets grow and assemble around the gas bubbles finally form the interesting $\alpha$-$Ni(OH)_2$ hollow spheres.

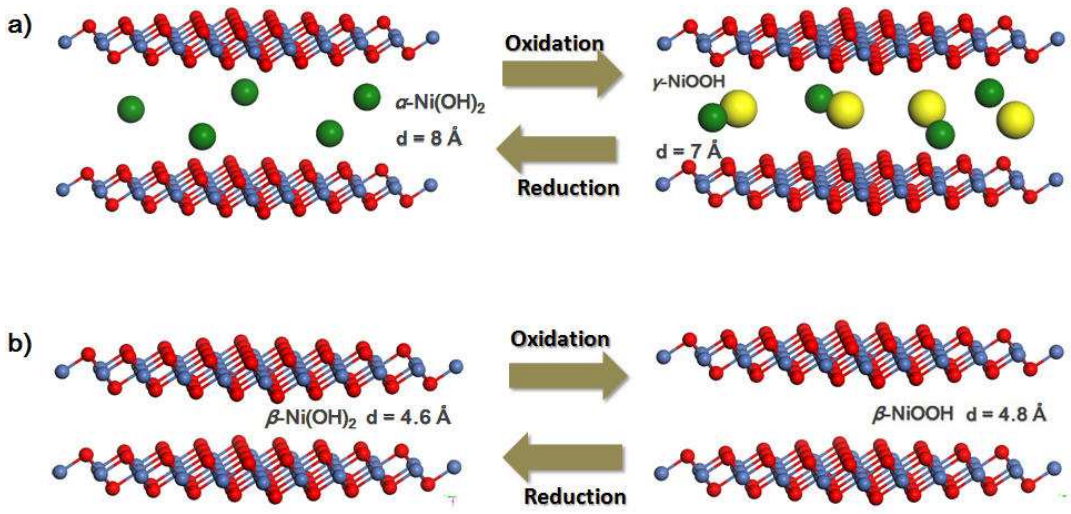


Figure S4. Structure transformation between nickel hydroxides and nickel oxyhydroxides. Blue and red balls correspond to Ni and O atoms, respectively. Large olive and yellow balls intercalated between the $NiO_2$ slabs correspond to water molecules and potassium ions. Hydrogen atoms are omitted for clarity in the structure.

It is well known that nickel hydroxide exists in two polymorphic forms, *i.e.*, $\alpha$-$Ni(OH)_2$ and $\beta$-$Ni(OH)_2$. The two forms crystallize in hexagonal system with $Ni(OH)_2$ layers stacked along the *c*-axis by slabs of edge-sharing $NiO_6$ octahedra. The $\alpha$-$Ni(OH)_2$ and $\beta$-$Ni(OH)_2$ can be easily oxidized to $\gamma$-NiOOH and $\beta$-NiOOH, respectively.[S2] In $\gamma$-NiOOH, edge-sharing $NiO_6$ octahedra are arranged into higher-order layers, which are interstratified with alkali cations and water molecules (Figure S4). For the short-range structure of $\beta$-NiOOH, it is suggested the presence of a Jahn-Teller distortion of the low-spin $d^7$ Ni(III) centers, which leads to an axial elongation and equatorial contraction of the oxygen ion ligand field.[S3]

We note that $\alpha$-$Ni(OH)_2$ is widely considered to have superior electrochemical properties than $\beta$-$Ni(OH)_2$, but it can transform easily to $\beta$-$Ni(OH)_2$ in strong alkaline solutions. However, recent new synthesis strategies afford $\alpha$-$Ni(OH)_2$ materials with new nanostructures, textural characteristics, and crystallite properties that lead to their excellent

stability in strong alkaline solutions.[S4-6] The $\alpha$-$Ni(OH)_2$ hollow spheres showed excellent stability in our tests and are promising for practical applications in various electrochemical energy devices.[S6]

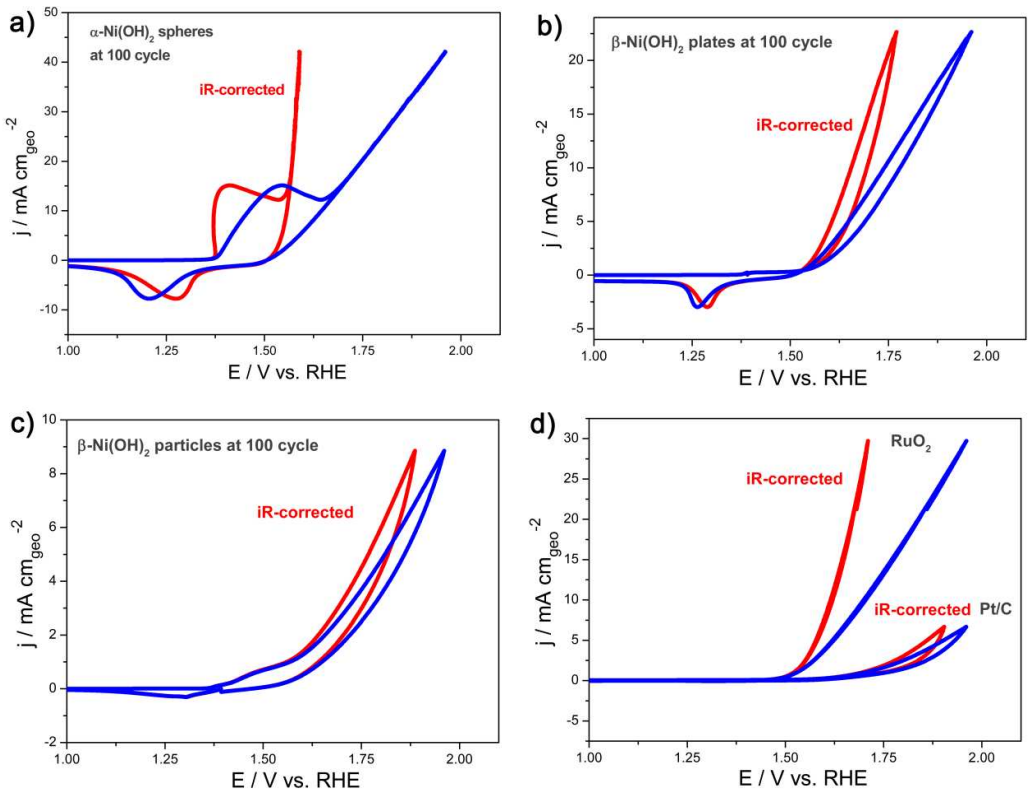


Figure S5. CVs recorded at 100$^{th}$ cycle for modified GC electrodes comprising the $\alpha$- and $\beta$-$Ni(OH)_2$ nanocrystals, $RuO_2$, and 20 wt% Pt/C with (red) and without (blue) iR correction. The ionic resistance (~44 Ω) from the solution was determined by the EIS technique.

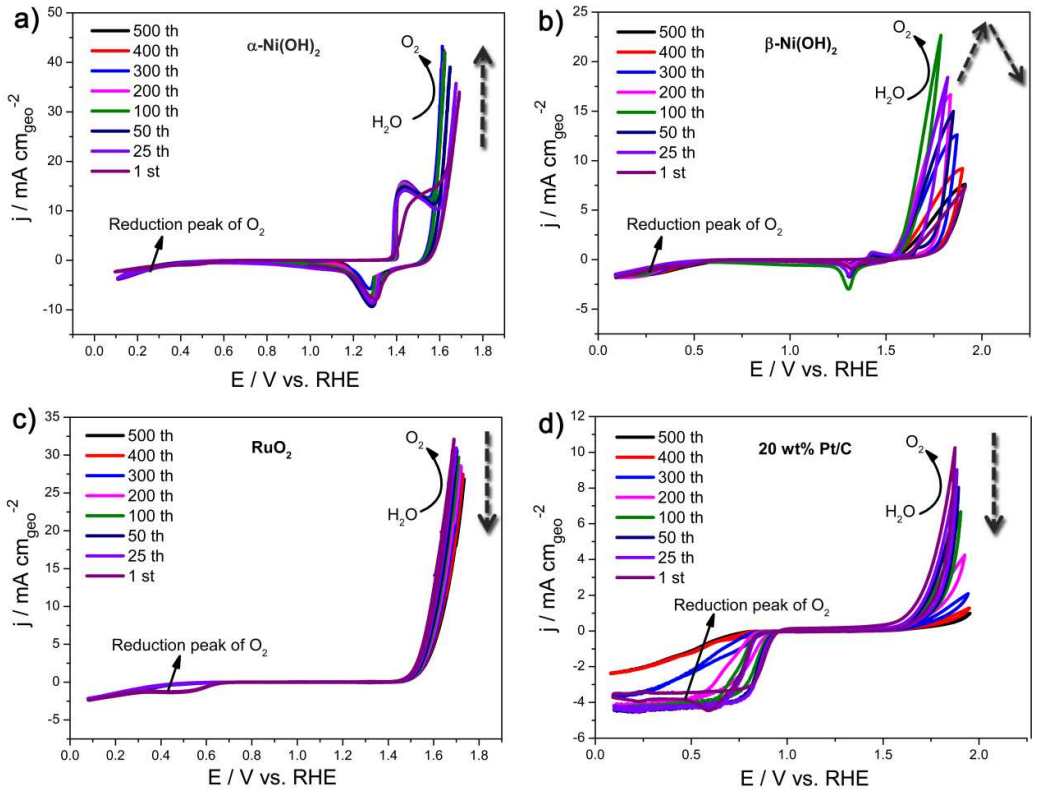


Figure S6. CV curves show the oxygen electrode activities within the oxygen reduction reaction (ORR) and oxygen evolution reaction (OER) potential window for (a) $\alpha$-$Ni(OH)_2$ hollow spheres, (b) $\beta$-$Ni(OH)_2$ nanoplates, (c) commercial $RuO_2$ catalyst, and (d) commercial Pt/C catalyst before and after different cycles of stability test in $O_2$-saturated 0.1 M KOH (pH ~13). CV curves were iR corrected. Catalyst loading: ~0.2 mg $cm^{-2}$. Sweep rate: 10 mV $s^{-1}$.

From Figure S6a and b, a small wave at about 0.4 V vs. RHE can be observed for both $\alpha$-$Ni(OH)_2$ and $\beta$-$Ni(OH)_2$ catalysts, corresponding to the reduction of oxygen. Such observation of ORR current is reminiscent of Lyons and co-workers' suggestions that nickel oxides could be used for the catalysis of the cathodic ORR.[S7] A slightly larger ORR catalytic current and higher onset potential are observed for commercial $RuO_2$ (Figure S6c). Of note, the ORR activities of $\alpha$-$Ni(OH)_2$, $\beta$-$Ni(OH)_2$ and $RuO_2$ are much lower than that of commercial Pt/C catalyst (Figure S6d). However, when the potential was extended to the water oxidation region, the $\alpha$-$Ni(OH)_2$ catalyst exhibits exceptional OER performance (including activity and stability), even better than commercial $RuO_2$ (Figure S6a-c). Pt/C

catalyst shows low OER activity, which along with its ORR activity decreases quickly under intensive CV cycling (Figure S6d).

**Table S1. Summary of Literature Tafel Slopes of Various Nickel-Based OER Catalysts.**

| Catalyst | Electrolyte | Tafel Slope (mV/decade) | Reference |
|---|---|---|---|
| $LaNiO_3$ | 1 M KOH | 43 | S8 |
| $LaNiO_3$ (containing $LaNiO_3$, $La_2NiO_4$, and NiO) | 1 M KOH | 65 | S8 |
| $Fe_{0.25}Ni_{0.75}MoO_4$ | 1 M KOH | 34±1/78±5 | S9 |
| $Ni_xCo_{3-x}O_4$ nanowire arrays | 1 M KOH | 59~64 | S10 |
| $NiB_i$ ($B_i$ = borate) | 0.1 M $H_2BO_3^-/H_3BO_3$ | 60 | S11 |
| $NiO_x$ (amorphous) | 0.1 M KOH | 73±6 | S12 |
| $FeNiO_x$ (amorphous) | 0.1 M KOH | 24±4 | S12 |
| $FeCoNiO_x$ (amorphous) | 0.1 M KOH | 31±3 | S12 |
| $\alpha$-$Ni(OH)_2$ | 0.1 M KOH | 42 | Present work |

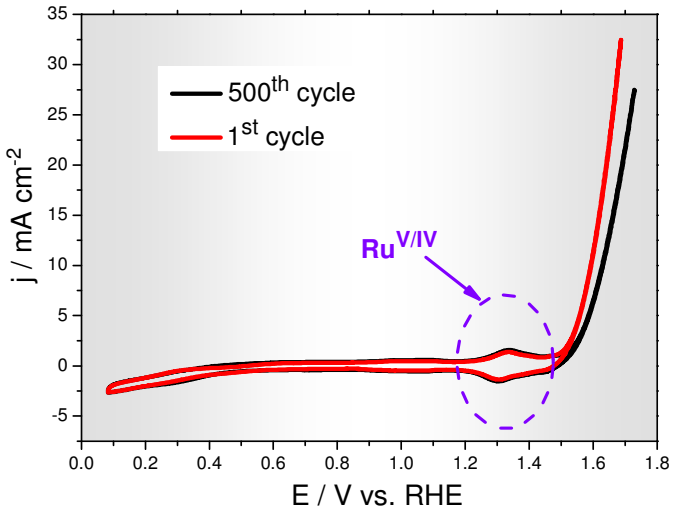


Figure S7. CVs recorded at 1st cycle and 500th cycle for commercial $RuO_2$ catalyst in $O_2$-saturated 0.1 M KOH at a large sweep rate of 250 mV $s^{-1}$. CV curves were iR corrected. Catalyst loading: 0.2 mg $cm^{-2}$.

Figure S7 shows the CV curves of commercial $RuO_2$ catalyst before and after stability tests at a high sweep rate of 250 mV $s^{-1}$, from which we can clearly observe a redox couple assigned to $Ru^{V/IV}$ between the potentials of 1.2 ~ 1.4 V vs. RHE,[S13] confirming to previous report that the high valent $Ru^{V}$ cations could be the active sites for catalyzing OER.[S14] Such a $Ru^{V/IV}$ redox couple is very similar to the $\alpha$-$Ni(OH)_2$/$\alpha$-NiOOH ($Ni^{IV/III}$) redox couple, all implying the highly oxidized metal sites may be intrinsically more active toward the OER.

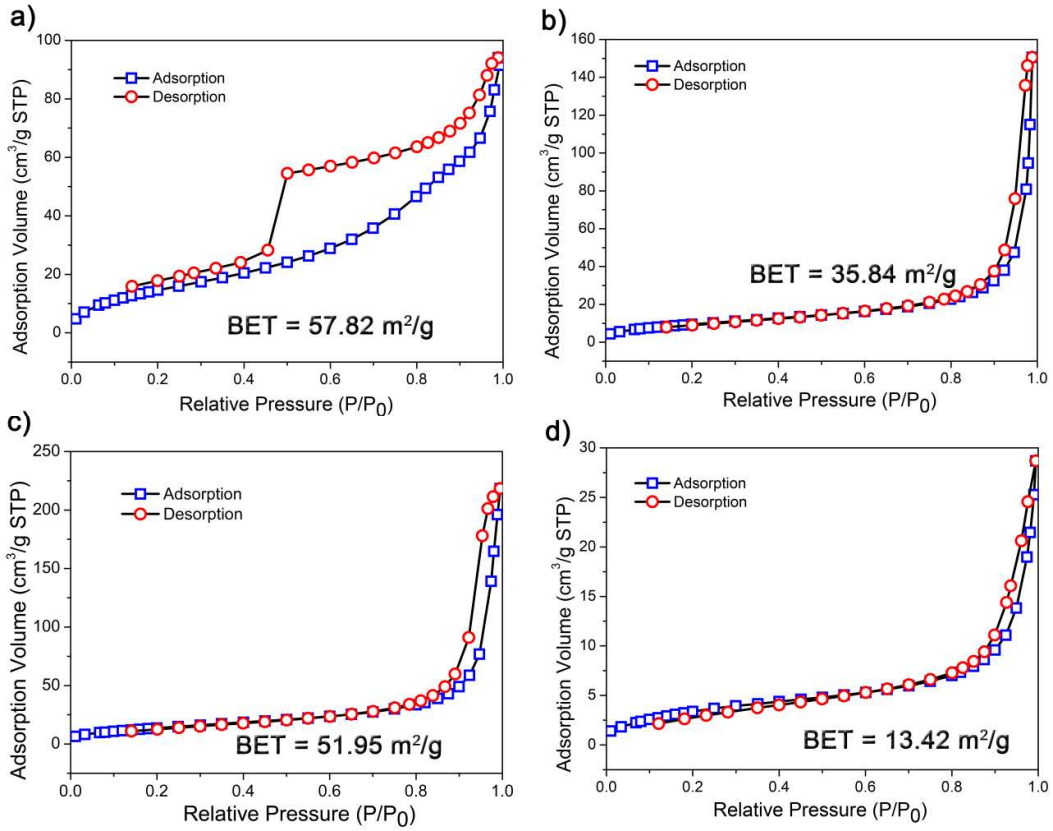


Figure S8. $N_2$ adsorption/desorption isotherms of (a) $\alpha$-$Ni(OH)_2$ hollow spheres, (b) $\beta$-$Ni(OH)_2$ nanoplates, (c) $\beta$-$Ni(OH)_2$ nanoparticles, and (d) commercial $RuO_2$ catalyst.

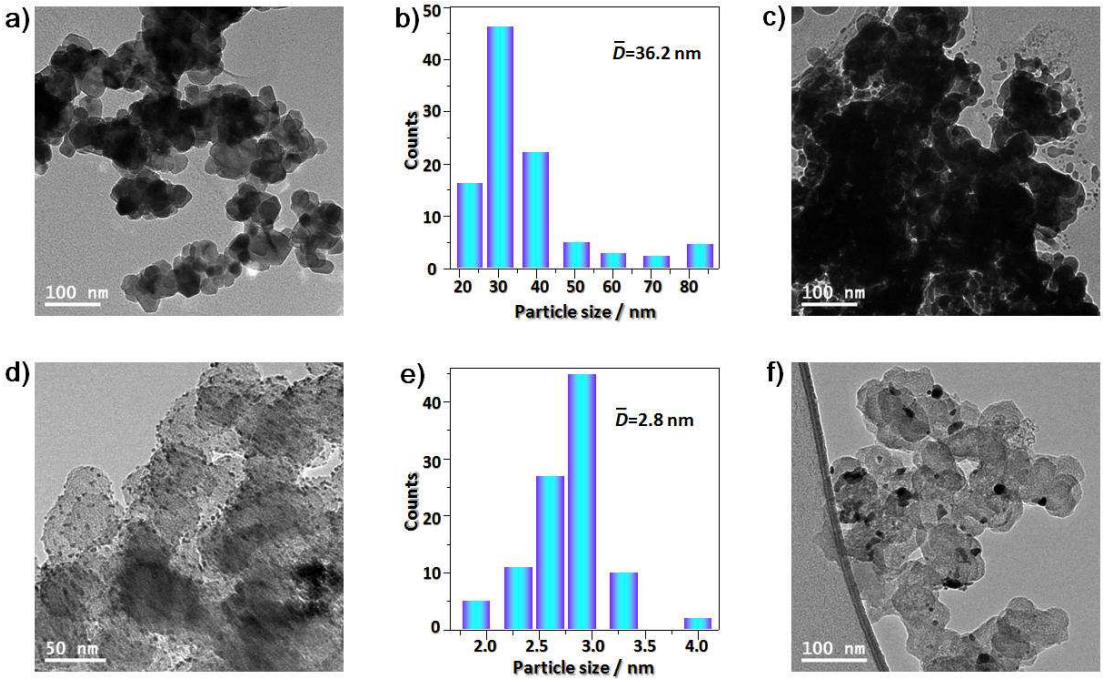


Figure S9. (a, d) TEM images taken before 500 cycles for commercial $RuO_2$ and Pt/C, respectively. (b, e) Average particle size histogram of commercial $RuO_2$ and Pt/C catalysts before 500 cycles, respectively, obtained from (a, d) by using Adobe Photoshop software. (c, f) TEM images taken after 500 cycles for commercial $RuO_2$ and Pt/C, respectively.

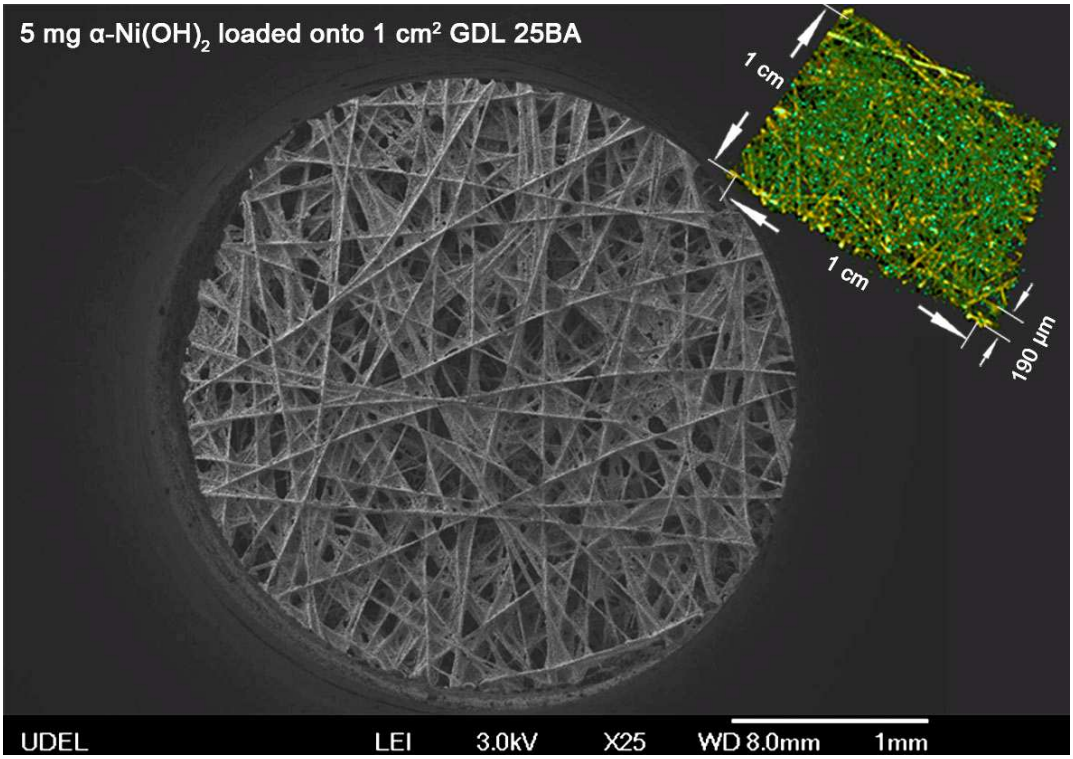


Figure S10. SEM image of the $\alpha$-Ni(OH)$_2$-modified-carbon fiber paper (CFP). The inset is the corresponding schematic representation of the $\alpha$-Ni(OH)$_2$ loaded CFP.

To evaluate the OER performance of $\alpha$-Ni(OH)$_2$ catalyst in real electrolysis, we deposited 5 mg $\alpha$-Ni(OH)$_2$ onto 1 cm$^2$ carbon fiber paper (CFP) uniformly by repeated dipping of CFP in $\alpha$-Ni(OH)$_2$ suspension until desired weight gain was reached. The CFP used here is gas diffusion layer (GDL 25BA) from SIGRACET® with thickness of 190 µm. The large pores among carbon fibers and also the three-dimensional structure of the CFP (Figure S10) make it is difficult to determine the real catalyst loading based on effective surface area. Therefore, we just used geometric area of CFP to represent the loading density of studied catalysts (*i.e.*, 5 mg cm$^{-2}$).

**Movie S1 ($O_2$ bubbles):**

This movie shows the $O_2$ evolution on $\alpha$-$Ni(OH)_2$ hollow spheres coated carbon fiber paper (CFP) electrode in the electrochemical cell at a moderate $\eta$ = 0.35 V. (electrolyte: 0.1 M KOH; $\alpha$-$Ni(OH)_2$ loading: 5 mg $cm^{-2}$)

## References:


(S1) Luo, Y. Y.; Li, G. H.; Duan, G. T.; Zhang, L. D. *Nanotechnology* **2006**, *17*, 4278.

(S2) Oliva, P.; Leonardi, J.; Laurent, J. F.; Delmas, C.; Braconnier, J. J.; Figlarz, M.; Fievet, F.; Deguibert, A. *J Power Sources* **1982**, *8*, 229.

(S3) Bediako, D. K.; Lassalle-Kaiser, B.; Surendranath, Y.; Yano, J.; Yachandra, V. K.; Nocera, D. G. *J. Am. Chem. Soc.* **2012**, *134*, 6801.

(S4) Jeevanandam, P.; Koltypin, Y.; Gedanken, A. *Nano Lett.* **2001**, *1*, 263.

(S5) Soler-Illia, G. J. d. A. A.; Jobbagy, M.; Regazzoni, A. E.; Blesa, M. A. *Chem. Mater.* **1999**, *11*, 3104.

(S6) Yan, J.; Fan, Z. J.; Sun, W.; Wei, T.; Zhang, Q.; Zhang, R. F.; Zhi, L. J.; Wei, F. *Adv. Funct. Mater.* **2012**, *22*, 2632.

(S7) Lyons, M. E. G.; Doyle, R. L.; Godwin, I.; O'Brien, M.; Russell, L. *J. Electrochem. Soc.* **2012**, *159*, H932.

(S8) Bockris, J. O.; Otagawa, T. *J Phys Chem-Us* **1983**, *87*, 2960.

(S9) Kumar, M.; Awasthi, R.; Pramanick, A. K.; Singh, R. N. *Int. J. Hydrogen Energ.* **2011**, *36*, 12698.

(S10) Dau, H.; Limberg, C.; Reier, T.; Risch, M.; Roggan, S.; Strasser, P. *ChemCatChem* **2010**, *2*, 724.

(S11) Dinca, M.; Surendranath, Y.; Nocera, D. G. *Proc. Natl. Acad. Sci.USA* **2010**, *107*, 10337.

(S12) Smith, R. D. L.; Prevot, M. S.; Fagan, R. D.; Zhang, Z. P.; Sedach, P. A.; Siu, M. K. J.; Trudel, S.; Berlinguette, C. P. *Science* **2013**, *340*, 60.

(S13) Wang, L.; Duan, L. L.; Stewart, B.; Pu, M. P.; Liu, J. H.; Privalov, T.; Sun, L. C. *J. Am. Chem. Soc.* **2012**, *134*, 18868.

(S14) Concepcion, J. J.; Tsai, M. K.; Muckerman, J. T.; Meyer, T. J. *J. Am. Chem. Soc.* **2010**, *132*, 1545.